JOURNAL OF MATERIALS SCIENCE 28 (1993) 3313–3321

Numerical analysis of the deformation and solidification of a single droplet impinging onto a flat substrate

C. SAN MARCHI, H. LIU, E. J. LAVERNIA, R. H. RANGEL
Department of Mechanical and Aerospace Engineering, University of California, Irvine, CA 92717, USA

A. SICKINGER, E. MUEHLBERGER
Electroplasma Inc., 16842 Milliken Ave., Irvine CA 92714, USA

An existing model has been modified to explore the deformation and solidification of a single droplet impinging on a substrate. The modification accounts for possible solid fraction of material at impact. Numerical results predict that the kinetic energy dominates the process at impinging velocities greater than about 100 $m\,s^{-1}$. In addition, the thermal diffusivity of the solidifying material controls the process, but the temperature of the substrate relative to the melting temperature of the material must be considered when comparing materials. It is believed that droplets solidifying into thinner, wider discs would reduce porosity; therefore, dense materials accelerated to high speed would solidify into masses with the highest bulk density.

Nomenclature

Properties and parameters

a_l	Thermal diffusivity of the liquid ($cm^2\,s^{-1}$)
a_s	Thermal diffusivity of the solid ($cm^2\,s^{-1}$)
b	Thickness of the molten metal (cm)
c_l	Specific heat of the liquid ($J\,g^{-1}\,K^{-1}$)
c_s	Specific heat of the solid ($J\,g^{-1}\,K^{-1}$)
D	Diameter of the droplet ($D = 2R_0$) (cm)
E_k	Kinetic energy (J)
E_p	Potential energy (J)
L_f	Work of the friction forces (W)
Δh	Enthalpy of fusion ($J\,g^{-1}$)
k_l	Thermal conductivity of the liquid ($W\,cm^{-1}\,K^{-1}$)
k_s	Thermal conductivity of the solid ($W\,cm^{-1}\,K^{-1}$)
R	Radius of the solidified disc (cm)
t^*	Real time (s)
τ^*	Real time from solidification (s)
T_l	Temperature of the molten metal (K)
T_m	Melting temperature (K)
T_s	Temperature of the substrate (K)
V_s	Volume of the solid (cm^3)
y	Thickness of the solidified layer (cm)
y_o	Thickness of the solidified layer at impact (cm)
μ	Viscosity of the molten metal ($mN\,s\,m^{-2}$)
χ	Mass fraction of the solid at impact
ρ_l	Density of the molten metal ($g\,cm^{-3}$)
ρ_s	Density of the solid metal ($g\,cm^{-3}$)
σ	Surface tension of the molten metal ($mN\,m^{-1}$)
ω	Velocity of the liquid droplet at impact ($cm\,s^{-1}$)

Dimensionless variables

t	Dimensionless time
τ	Dimensionless time from solidification
T_o	Dimensionless temperature of the substrate
T_p	Dimensionless temperature of the droplet
ϕ	Dimensionless thickness
ξ	Dimensionless radius
Pe	Peclet number
Re	Reynolds number
We	Weber number

Constants

κ	Constant (Equation 13)
ε	Constant ($=0.5$)
U	Freezing constant (Equation 1)

1. Introduction

In an effort to optimize the structure and properties of structural materials, a variety of processing techniques have evolved over the last two decades. Among these, spray processes offer a unique opportunity to combine the benefits associated with fine-particulate technologies (e.g. microstructural refinement, alloy modifications, etc.) with *in situ* processing and, in some cases, near-net shape manufacturing. Spray processing generally involves highly non-equilibrium thermal and solidification conditions, the synthesis approach of which allows modification of the properties of existing alloy systems and the development of novel alloy compositions. There exists a variety of spray-based synthesis methods currently available. These include low-pressure plasma deposition [1, 2], modified gas-welding techniques [3, 4], high-velocity oxyfuel thermal spraying [5] and spray atomization and depos-

0022–2461

ition processing [6–9]. Plasma processing, in particular, has been extensively developed as a cost-effective method of producing metallic and refractory coatings on bulk shapes [10, 11].

The microstructure and meehanical properties of metals and alloys processed by spray techniques are intimately coupled to the kinetic, thermal and solidification conditions of the droplets during impact with the target surface. In spray atomization and deposition processes, for example, an elevated volume fraction of solid on impact, generally leads to the formation of a large volume fraction of porosity [12]. Similarly, extensive pre-solidification during plasma spraying causes poor bonding between the coating and the substrate [13, 14]. Therefore, it is not surprising that a number of investigators have utilized mathematical modelling techniques to provide insight into fundamental kinetic, thermal and solidification phenomena during spray processing [15–17]. Inspection of the published literature, however, demonstrates that despite the significant results derived from these models, the studies have not addressed the fundamental problem posed by the impact, deformation and solidification of a single droplet impinging on to a target surface. Therefore, the present study was devoted to the numerical analysis of the deformation and solidification of a single droplet impinging on a hard, non-deformable surface without addressing the physics of the flight stage. The numerical study was conducted for several pure metals at different processing parameters. Moreover, in the present work, the effect of a fraction of solid material within the droplet at impingement with the substrate is investigated. This condition is typical in plasma processing and spray atomization and deposition where droplets may partially solidify before impact due to high heat-transfer rates during flight. However, a second mechanism, insufficient residence time of particles in the plasma flame resulting in incomplete melting, makes solid fraction analysis particularly important for plasma processes.

2. Formulation

Characterizing the solidification and motion of a droplet impinging on a flat horizontal, non-deformable surface requires solution of the Navier–Stokes and energy equations. However, Madejski [18] has developed a simple model for the motion and solidification of a droplet on a surface based on an energy balance. Madejski's equations are solved for one-dimensional half-space heat conduction and solidification of superheated liquid. The physics of impact are related to the velocity and shape of the impacting droplet. In real spray systems, a droplet may break apart into smaller splats on impact, translating momentum to the smaller splats. However, this model assumes that the droplet remains as one mass of liquid that translates its momentum radially without any initial kinetic losses to the surroundings. It is also assumed that the droplet forms a cylinder on impact and the liquid spreads uniformly with the solidification front growing from the substrate–liquid interface to the exposed surface of the droplet. These assumptions imply solidification of the droplet into a thin flat disc. Furthermore, these geometrical considerations are made to limit the complexity in generating the necessary equations to describe the deformation and solidification of the droplet. Nonetheless, sprayed droplets are typically found to form very thin discs during solidification.

The model originally developed by Madejski does not account for partial solidification during flight; however, as described previously, partial or complete solidification during flight in spray processing may be significant. In the present study we have modified Madejski's model to consider the case of partial solidification before impact. Upon impact it is assumed that the solidified material has an interface varying only radially from a maximum at the centre of the cylinder to zero at the initial radius of the droplet (Fig. 1). The liquid cylinder becomes distorted due to the varying thickness of the solidified layer, unless the solid layer is very thin. If the solid layer thickness does not significantly vary radially, the approximation $b(r, t^*) \approx b(t^*)$ becomes valid, where b is the thickness of the liquid layer, r is the radial position, and t^* is the real time. Therefore, if the solid fraction at impact is small (< 0.4), the volume of solidified metal is independent of the radial position.

The Stefan problem for solidification as described by Madejski is modified for radial positions, r, less than the initial radius of the spherical droplet, R_0, ($r < R_0$) such that

$$y(r, t^*) = y_0(r) + U(a_s t^*)^{1/2} \quad (1)$$

where $y(r, t^*)$ is the thickness of the solidified layer at any real time after impact ($t^* > 0$), $y_0(r)$ is the radial variation of the thickness of the solidified layer at impact (equal to zero in the Madejski model), U is the freezing constant, and a_s is the thermal diffusivity of the solid layer (Fig. 2). The thickness of the solidified layer for radial positions greater than the initial radius of the spherical droplet ($r > R_0$) remains the same in

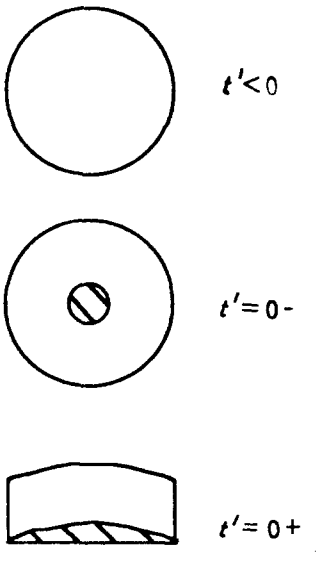

Figure 1 Partial solidification of droplet before impact.

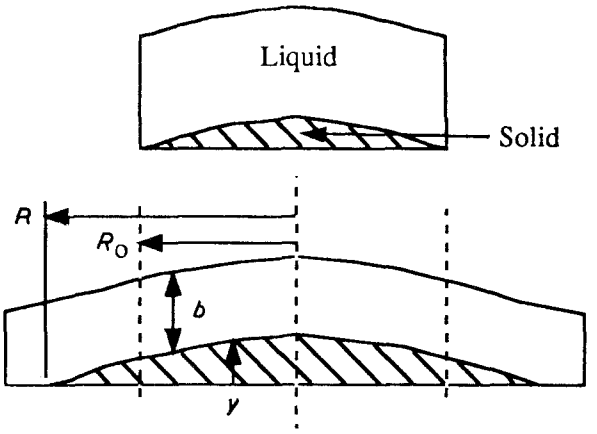

Figure 2 The growth of the solidified disc.

the modified model as in the original Madejski model

$$y(r, t^*) = y_o(r) + U[a_s(t^* - \tau^*)^{1/2} \quad (2)$$

where τ^* is the time that solidification begins at some position r. The remainder of the model is the same as Madejski's original model incorporating the revised thickness of the solidified layer (equation 1) into the equation development.

Madejski suggested that an energy balance for the motion of the liquid metal after impact has three components: E_k, the kinetic energy; E_p, the potential energy (due to surface tension); and L_f, the work of the friction forces. Conservation of energy implies that the total energy must be constant with time; therefore

$$\frac{d}{dt^*}(E_k + E_p + L_f) = 0 \quad (3)$$

Madejski's manipulations produce the following relations for the three energy components

$$E_k = \frac{\pi}{3}\rho_l\left(\frac{dR}{dt^*}\right)^2\left(bR^2 + \frac{6}{5}b^3\right) \quad (4)$$

$$E_p = \sigma(\pi R^2 + 2\pi Rb) \quad (5)$$

$$L_f = \int_0^{t^*} \frac{\pi R^2 \mu}{b}\left(\frac{dR}{dt^*}\right)^2 dt^* \quad (6)$$

where ρ_l is the density of the liquid, $R(t^*)$ is the radius of the solidified disc, σ is the surface tension of the liquid, and μ is the viscosity of the liquid. The potential energy relation cannot be satisfied at time zero; however, if the initial radius of the cylinder is assumed to be half the diameter of the droplet, an error of only 8% occurs at time zero [18]. The relation

$$R(0) = R_o = \varepsilon D \quad (7)$$

is introduced to account for this assumption where D is the diameter of the original spherical droplet and ε is a constant equal to one-half. By introducing the following dimensionless variables

$$\xi = R/R_o \quad (8a)$$

$$\phi = b/R_o \quad (8b)$$

$$t = \omega t^*/R_o \quad (8c)$$

and the Peclet, Reynolds, and Weber numbers

$$Pe = \omega D/a_s \quad (9a)$$

$$Re = \rho_l \omega D/\mu \quad (9b)$$

$$We = \rho_l \omega^2 D/\sigma \quad (9c)$$

in Equations 4–7, we can rewrite Equation 3 as

$$\frac{d}{dt}\left[\frac{\varepsilon}{3}\dot{\xi}^2\phi\left(\xi^2 + \frac{6}{5}\phi^2\right) + \frac{1}{We}\xi(\xi + 2\phi)\right] + \frac{\xi^2\dot{\xi}^2}{\phi Re} = 0 \quad (10)$$

where ω is the velocity of the liquid droplet at impact. The dimensionless thickness, ϕ, can be determined from a mass balance

$$m = \frac{\pi}{6}D^3\rho_l = \rho_s V_s + \pi R^2 b\rho_l \quad (11)$$

where m is the mass of the droplet, ρ_s is the density of the solid, and V_s is the volume of the solid. Recognizing that $r = R(\tau^*)$ and applying Equations 1 and 2, the volume of the solid becomes

$$V_s = \pi R_o^2 U(a_s t^*)^{1/2} + \int_0^{t^*} 2\pi R(\tau^*)\frac{dR(\tau^*)}{d\tau^*}y_o(R)d\tau^* + \int_0^{t^*} 2\pi R(\tau^*)\frac{dR(\tau^*)}{d\tau^*}U[a_s(t^* - \tau^*)]^{1/2}d\tau^* \quad (12)$$

Solving for the thickness of the liquid layer from Equation 11, applying the previously specified dimensionless parameters, and introducing the parameter κ, such that

$$\kappa = 6\varepsilon^2 U\frac{\rho_s}{\rho_l}\left(\frac{\varepsilon}{Pe}\right)^{1/2} \quad (13)$$

the dimensionless thickness becomes

$$\phi = \frac{1}{6\varepsilon^2\xi^2}\left(1 - \chi - \kappa\left\{t^{1/2} + 2\int_0^t \xi(\tau)\dot{\xi}(\tau) \times (t - \tau)^{1/2}d\tau\right\}\right) \quad (14)$$

where χ is the mass fraction of the solid at impact. Applying the condition $t = 0$ the initial boundary conditions for this set of equations become

$$\xi(0) = 1$$

$$\phi(0) = \frac{4}{3} - \chi \quad (15)$$

$$\dot{\xi}(0) = \left[3/2\Big/\left(1 + \frac{1}{30\varepsilon^6}\right)\right]^{1/2}$$

The freezing constant, U, is determined from the Stefan problem of solidification as described by Madejski and has the following form

$$U = \frac{2}{\pi^{1/2}}\left(\left[T_0\Big/\left(\operatorname{erf}\frac{U}{2}\right)\exp\left(\frac{U^2}{4}\right)\right] - \left\{T_p\left(\frac{(kc\rho)_l}{(kc\rho)_s}\right)^{1/2}\Big/\operatorname{erfc}\left[\frac{U}{2}\left(\frac{a_s}{a_l}\right)^{1/2}\right] \times \exp\left(-\frac{U^2 a_s}{4a_l}\right)\right\}\right) \quad (16)$$

where k, c, and a are the thermal conductivity, the heat capacity, and the thermal diffusivity, respectively, of the liquid or solid as denoted by the subscripts l for liquid and s for solid. The variables T_o and T_p are the dimensionless temperature of the substrate and the dimensionless temperature of the droplet, respectively, and they have the form

$$T_o = \frac{k_s(T_{mp} - T_s)}{a_s \rho_s \Delta h} \quad (17a)$$

$$T_p = \frac{k_s(T_l - T_{mp})}{a_s \rho_s \Delta h} \quad (17b)$$

where T_{mp}, T_s, and T_l, are the melting temperature, the substrate temperature and the liquid temperature respectively and Δh is the enthalpy of fusion [18]. It is important to reiterate that Equation 16 is valid for the isothermal case which assumes that the solidified metal is the same temperature as the substrate. Madejski's experimental observations have concluded that this approximation is satisfied regardless of the substrate material [18].

3. Computational method

The system of equations developed above is numerically solved as shown in Fig. 3a and b. The dimensionless parameters (Re, We, Pe, T_o, T_p) were determined by substituting the properties of the pure solid and liquid metals at the chosen temperatures and the chosen parameters (velocity, droplet size, etc.) into Equations 9 and 17. Initially, a value for the freezing constant was assumed and the error functions in Equation 16 were interpolated at steps of 0.05. A new value for the freezing constant can be found by substituting these values and the appropriate properties into the right side of Equation 16. Comparing the calculated value of the freezing constant with the assumed value, a new value of the freezing constant was

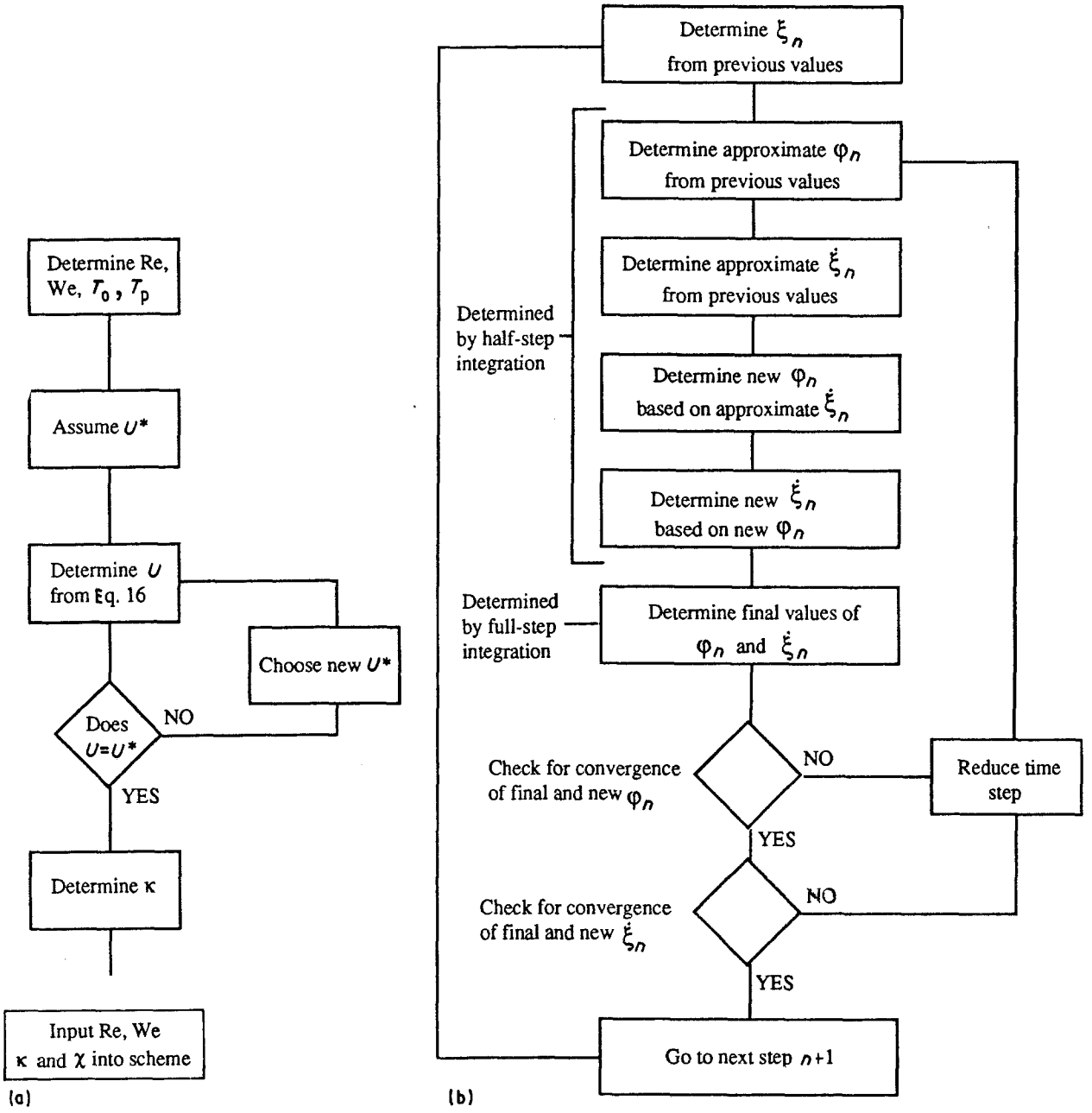

Figure 3 (a) Determination of the dimensionless parameter κ. (b) Schematic of steps taken to solve Equations 10 and 14.

approximated. This process was repeated until the assumed value of the freezing constant matched the value of the freezing constant determined from Equation 16 as shown in Fig. 3a. Determining the dimensionless parameter, κ, Equation 13, is trivial once the freezing constant has been determined.

The dimensionless parameters (specifically Re, We, κ, and χ) are used to evaluate a scheme designed to solve Equations 10 and 14 simultaneously. The form of the dimensionless thickness of the liquid, Equation 14, is an integro-differential equation that depends on the dimensionless radius and its first time derivative (ξ and $\dot{\xi}$). A predicted value of $\dot{\xi}$, determined from a standard Runge–Kutta scheme, is used to find the value of the corrected dimensionless thickness, ϕ, and subsequently a corrected value of $\dot{\xi}$. Using the above outlined procedure, the system of equations can be solved at the new time step, producing values for the dimensionless radius and its derivative and the dimensionless thickness (Fig. 3b). Therefore, the equations can be solved by stepping through time.

We should reiterate that this model breaks down for large solid fractions, typically above 40%–50% solid. From Equation 14 it is obvious that the solid fraction will reach a critical value that causes ϕ to be negative which is physically impossible. The profile of the solid fraction at impact has no effect on the equations if, as described previously, $y_0(r)$ is assumed to be thin such that $b(r, t^*) \approx b(t^*)$. Thus the present model is numerically valid for solid fractions less than about 0.40.

4. Results and discussion

The deformation and solidification history of a single droplet of nickel, titanium, and tungsten was numerically determined. The processing parameters were varied for each metal, namely temperature of the molten metal, and the substrate, velocity, size of the initial droplet, and solid fraction at impact. The processing parameters for investigation were chosen to be characteristic of typical low-pressure plasma spray (LPPS) processing conditions, because of the recent interest in this processing technique. For example, LPPS operates at velocities on the order of a few hundred metres per second; therefore, we chose to concentrate on a velocity range from 100–900 $m\,s^{-1}$. Similarly, the droplet size was varied from 25–100 μm, again typical powder sizes for powder spraying techniques. The temperature of the substrate was arbitrarily chosen at high temperatures (750, 1000, 1250 K, etc.) because typical LPPS procedures use the plasma torch to clean the substrate before deposition, thus significantly heating the substrate. Superheat temperatures were chosen to be 100 and 250 K above the melting temperature, strictly for convenience. The properties of these materials at various temperatures are listed in Tables I and II [19–21]. The results are summarized in Figs 4–9.

Droplet flattening (the formation of a solidifying disc with a large radius) is significantly dependent on its velocity, especially at low velocities ($< 100\ m\,s^{-1}$). Fig. 4 shows the dimensionless radius as a function of the velocity over a large velocity range, 1–2000 $m\,s^{-1}$ for tungsten. Above 500 $m\,s^{-1}$ the solidified droplet size begins to level off and approaches some asymptotic value at very large velocities ($> 5000\ m\,s^{-1}$). However, this model is not adequate to describe the physics at such large velocities, because during actual processing, molten droplets with large velocities will break up into smaller splats at impact.

Fig. 5 compares the velocity dependence of the flattening of nickel, titanium, and tungsten droplets at substrate temperatures of 1000 and 1500 K. The velocity dependence curves at different temperatures have identical shapes for all the materials converging at low velocities ($< 50\ m\,s^{-1}$). At higher velocities, the flattening of each material approaches an asymptotic value that is characteristic of that material and depends slightly (typically 1%–5% over a temperature range of 500 K) on the substrate temperature. However, as the melting point is approached the substrate temperature becomes increasingly important to the final size of the solidified disc as shown in Fig. 5 for tungsten and Fig. 6 for nickel. Tungsten forms flatter, wider discs than the other materials as shown by its large characteristic dimensionless radius, > 12 at 900 $m\,s^{-1}$, while titanium forms significantly smaller discs at 900 $m\,s^{-1}$, dimensionless radius of ~ 10. The characteristic radius of each material is unique and

TABLE I Properties of solid nickel, titanium, and tungsten at several temperatures

		Temperature (K)				
		1000	1250	1500	2900	3400
Nickel	Thermal diffusivity ($cm^2\,s^{-1}$)	0.150	0.155	0.160		
	Thermal conductivity ($W\,cm^{-1}\,K^{-1}$)	0.718	0.772	0.825		
	Heat capacity ($J\,g^{-1}\,K^{-1}$)	0.557	0.588	0.620		
Titanium	Thermal diffusivity ($cm^2\,s^{-1}$)	0.069	0.080	0.082		
	Thermal conductivity ($W\,cm^{-1}\,K^{-1}$)	0.207	0.224	0.245		
	Heat capacity ($J\,g^{-1}\,K^{-1}$)	0.695	0.618	0.660		
Tungsten	Thermal diffusivity ($cm^2\,s^{-1}$)	0.417	0.381	0.353	0.266	0.251
	Thermal conductivity ($W\,cm^{-1}\,K^{-1}$)	1.208	1.137	1.087	0.915	0.898
	Heat capacity ($J\,g^{-1}\,K^{-1}$)	0.150	0.156	0.162	0.200	0.215

TABLE II Properties of liquid nickel, titanium, and tungsten at T_{mp} and T_{mp} + 100 K

Property	Temperature = T_{mp}			Temperature = T_{mp} + 100 K		
	Nickel	Titanium	Tungsten	Nickel	Titanium	Tungsten
Thermal diffusivity ($cm^2 s^{-1}$)	0.116	0.070	0.174	0.117	0.071	0.178
Thermal conductivity ($W cm^{-1} K^{-1}$)	0.600	0.200	0.706	0.600	0.200	0.713
Capacity heat ($J g^{-1} K^{-1}$)	0.656	0.700	0.230	0.656	0.700	0.230
Density ($g cm^{-3}$)	7.905	4.110	17.60	7.789	4.040	17.45
Viscosity ($mN s m^{-2}$)	5.486	5.200	3.000	4.530	5.200	3.000
Surface tension ($mN m^{-1}$)	1778	1650	2500	1740	1624	2471

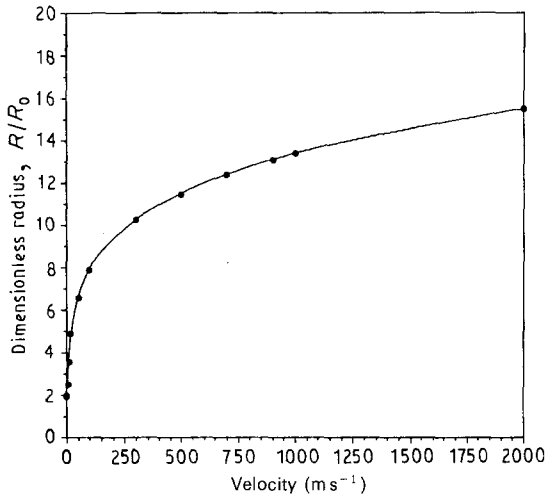

Figure 4 The velocity dependence of the droplet size of tungsten over a wide range of velocities. T_s = 2000 K, T_l = 3650 K, R_0 = 50 μm.

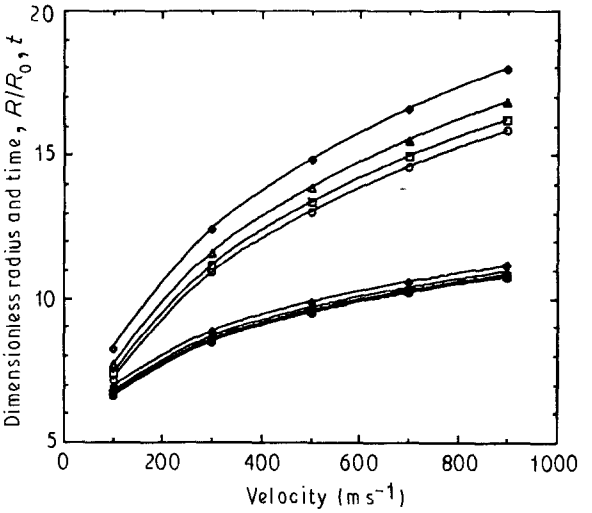

Figure 6 Comparison of the sensitivity of the solidification time and droplet flattening to velocity and substrate temperature for nickel. $T_l = T_{mp}$, R_0 = 50 μm. (○, □, △, ◇) Time, (●, ■, ▲, ◆) R/R_0. T_s: (○, ●) 750 K, (□, ■) 1000 K, (△, ▲) 1250 K, (◇, ◆) 1500 K.

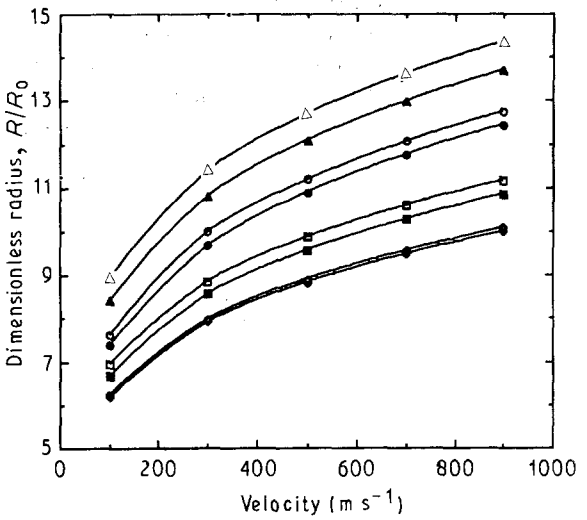

Figure 5 Flattening sensitivity to velocity and substrate temperatures. R_0 = 50 μm, $T_l = T_{mp}$. T_s = 1000 K: (●) W, (■) Ni, (◆) Ti. T_s = 1500 K: (○) W, (□) Ni, (◇) Ti. T_s = 2900 K: (▲) W. T_s = 3400 K: (△) W.

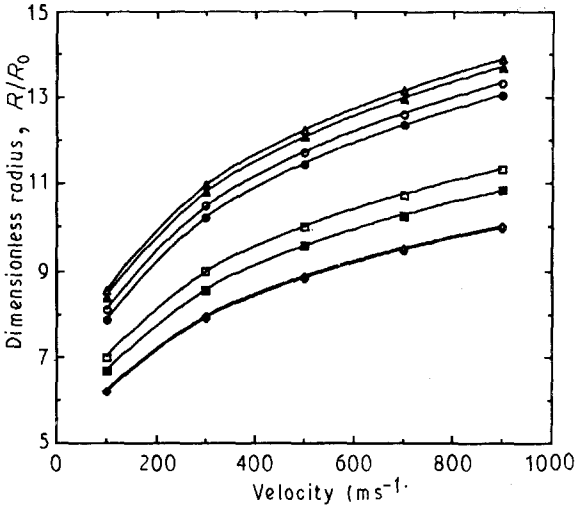

Figure 7 Flattening sensitivity to velocity and superheating. R_0 = 50 μm, T_s = 2000 K for W, 2900 K for W*, and 1000 K for Ni and Ti. W: T_l = (●) 3650 K = T_{mp}, (○) T_{mp} + 100 K; W*: T_l = (▲) 3650 K = T_{mp}, (△) T_{mp} + 100 K; Ni: T_l = (■) 1727 K = T_{mp}, (□) T_{mp} + 100 K; Ti: (◆) 1958 K = T_{mp}, (◇) T_{mp} + 100 K.

depends on the density of the material. Denser materials have a greater kinetic energy (for the same size or volume) than less-dense materials. Recall that the potential energy is independent of density; it is based on the surface tension of the droplet, representing the resistance of the molten metal to spreading or flattening. Therefore, the increased kinetic energy of denser materials overcomes the potential energy, forming wider, thinner solidified discs. As a result, dense materials such as tungsten are expected to flatten into wider discs relative to low-density materials such as titanium.

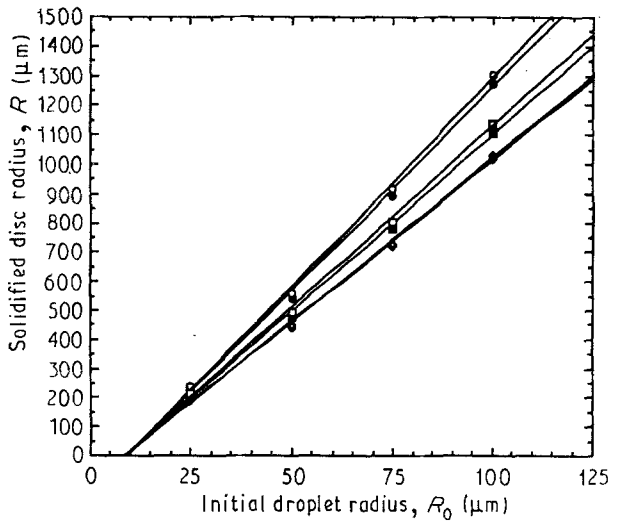

Figure 8 Flattening sensitivity to initial droplet size and substrate temperature. Velocity = 500 m s^{-1}, $T_l = T_{mp}$. T_s: (●) W, 1000 K; (■) Ni, 1000 K; (◆) Ti, 1000 K; (○) W, 1500 K; (□) Ni, 1500 K; (◇) Ti, 1500 K.

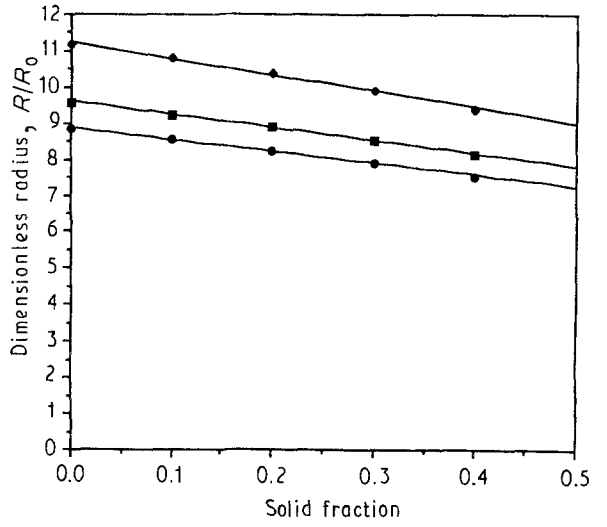

Figure 9 Dimensionless radius as a function of the solid fraction. $T_l = T_{mp}$, $T_s = 1000$ K, $R_0 = 50$ μm, velocity = 500 m s^{-1}. (●) Ti, (■) Ni, (◆) W.

Furthermore, as shown in Fig. 5, the sensitivity of solidification to the substrate temperature varies for these materials. For example, the flattening of a titanium droplet increases less than 1% when the temperature is raised from 1000 K to 1500 K at 900 m s^{-1}. The flattening of nickel and tungsten is slightly more sensitive to temperature than titanium; the size of a tungsten droplet increases 2.5%–3.5% and the size of a nickel droplet increases 3%–4% for the same temperature change (1000 K to 1500 K) over the range of velocities investigated (100–900 m s^{-1}). Although the solidification process is a complex combination of the properties of the liquid and solid material, in general, the thermal diffusivity seems to govern the temperature sensitivity of these materials. Titanium has a small thermal diffusivity and, therefore, a small temperature dependence. On the other hand, nickel has a significantly greater thermal diffusivity, accounting for its much larger temperature sensitivity. Tungsten would then be expected to have a greater sensitivity to temperature than nickel, although Fig. 5 shows otherwise in the same temperature range (1000–1500 K). This observation may be attributed to the fact that this temperature range is near the melting point of nickel (1727 K) and titanium (1958 K), while the melting point of tungsten is some 2000 K greater than this range (3650 K). Fig. 5 also shows the velocity dependence of tungsten in a temperature range that is 250–750 K less than its melting point (2900–3400 K); this temperature range is similar to the temperature range relative to the melting temperature for nickel and titanium. In this temperature range tungsten behaves according to our previous observation; tungsten has a larger sensitivity to substrate temperature due to its larger thermal diffusivity. These observations emphasize the importance of considering the temperature relative to the melting point of a material in addition to absolute temperature considerations, especially when comparing low melting materials and high melting materials.

In Fig. 7 we observe a perturbation of the trends illustrated by varying the substrate temperature. The sensitivity of the materials to superheating is qualitatively similar to the sensitivity of the materials to substrate temperature described above, except that despite its larger thermal diffusivity tungsten is less sensitive to superheat. For example, titanium is relatively insensitive to superheating. However, by comparison, nickel is extremely sensitive to superheat temperatures, for a superheat of 100 K the flattening increases by 4%–5% in the velocity range of interest (with a substrate temperature of 1000 K and an initial droplet size of 50 μm). Tungsten is only moderately affected by superheat, increasing its solidified droplet size by 2%–3% for the same conditions except with a substrate temperature of 2000 and 2900 K. This can be explained by the properties used for the analysis. Superheating nickel reduces its viscosity allowing it to spread with less resistance; therefore, the flattening of the droplet is enhanced by superheating. There are no data available for the viscosity of tungsten liquid as a function of temperature, thus we assumed that the viscosity was constant. Although the viscosity of tungsten probably decreases with superheat, our results do not reflect the enhanced flattening due to this phenomenon.

At present we are not interested in the time for complete solidification, although we briefly describe it here because the time can become important to phase formation in droplets especially in alloy systems. The time (dimensionless) for solidification varies more than the size with changes in the parameters for all the materials investigated; Fig. 6 compares the dimensionless time with the dimensionless radius for nickel. For example, as described previously, the size of a nickel droplet increases as much as 5% when the substrate temperature is increased from 1000 K to 1500 K, but the dimensionless time increases by as much as 12% for the same step in temperature. The actual time for solidification is of the order of microseconds, 0.1–10 μs. However, it must be kept in mind that the dimensionless time depends directly on the velocity

TABLE III Dimensionless and actual time for solidification of nickel[a]

Velocity ($m s^{-1}$)	Substrate temperature = 1000 K		Substrate temperature = 1500 K	
	Dimensionless time, t	Actual time, t^* (μs)	Dimensionless time, t	Actual time, t^* (μs)
100	7.38	3.69	8.26	4.13
300	11.19	1.86	12.45	2.08
500	13.38	1.34	14.85	1.48
700	14.96	1.07	16.60	1.19
900	16.21	0.90	17.98	1.00

[a] The molten metal temperature was the appropriate melting temperature, and the initial droplet size was 50 μm.

(see Equation 8). Therefore, the actual time decreases as the velocity is increased, even though the dimensionless time increases. For example, for nickel the actual time decreases by approximately a factor of four over the velocity range of 100–900 $m s^{-1}$, while the dimensionless time increases by a factor of two (T_s = 1500 K, $T_l = T_{mp}$ = 1727 K, and R_o = 50 μm). Table III summarizes this phenomenon for nickel. Conceptually the droplet is expected to freeze faster at higher velocities because the droplet has more energy to spread faster and expose more surface area to the cooler substrate.

The sensitivity of droplet flattening to velocity can be more important than the temperature dependence, especially for materials at temperatures much lower than the melting temperature and for materials with low thermal diffusivity such as titanium. To quantify and compare the velocity dependence of the various materials, Table IV lists the ratio of the change in size of the solidified droplet as a percentage to the change in velocity also as a percentage ($\Delta\xi/\xi/\Delta\omega/\omega$). For titanium and nickel the ratio of percent change in size to percent change in velocity ranges from 0.14–0.19 as the velocity is varied from 100–900 $m s^{-1}$, while for tungsten this parameter changes from 0.16 to 0.20 at the same temperature (1500 K). However, adjusting the tungsten temperature to represent an equivalent temperature relative to the melting temperature (3400 K) as nickel, this parameter has similar values for tungsten as nickel and titanium. These numbers show that the velocity dependence of solidification is virtually independent of the specific material. This phenomenon occurs because the properties of the material are independent of the velocity, thus all materials behave similarly with respect to the velocity. However, the properties of the material are dependent on temperature and can greatly influence the solidification; thus, as we have demonstrated, materials behave differently based on temperature, but similarly based on velocity.

TABLE IV Change in solidifed droplet size for changes in velocity[a]

Δ Velocity ($m s^{-1}$)	(% Δξ)/(%Δω)			
	Nickel	Titanium	Tungsten	
			1500 K	3400 K
100–300	0.138	0.140	0.156	0.139
300–500	0.172	0.172	0.177	0.172
500–700	0.183	0.182	0.195	0.183
700–900	0.188	0.187	0.200	0.188

[a] For all materials the substrate temperature was 1500 K (except where noted), the molten metal temperature was the appropriate melting temperature, and the initial droplet size was 50 μm.

The sensitivity of droplet flattening to initial droplet size is similar to the velocity sensitivity, because the material properties are independent of the droplet size. The data shown in Fig. 8 for superheated materials support our conclusions previously drawn from the velocity data at various substrate temperatures. However, we should note that doubling the initial radius of the droplet does not simply double the final size of the droplet. For example, when the initial size of a titanium droplet is doubled from 25 μm to 50 μm, the dimensionless radius increases 15.6%, but the actual droplet size increases 131% (at a velocity of 500 $m s^{-1}$). These values are very similar for all three materials as shown in Table V and are independent of the material. In addition, just as the materials behave

TABLE V The actual change in the solidified droplet size for changes in the initial droplet size[a]

ΔR_o (μm)	Nickel		Titanium		Tungsten T_S = 1500 K		Tungsten T_S = 3400 K	
	%Δξ	%ΔR	%Δξ	%ΔR	%Δξ	%ΔR	%Δξ	%ΔR
25–50	15.7	131	15.6	131	17.2	134	15.7	131
50–75	8.82	63.2	8.77	63.2	9.46	64.2	8.83	63.2
50–100	15.5	131	15.4	131	19.1	138	15.5	131
75–100	6.15	41.5	6.11	41.5	8.76	45.0	6.16	41.5

[a] For all materials the substrate temperature was 1500 K (except where noted), the molten metal temperature was the appropriate melting temperature, and the velocity was 500 $m s^{-1}$.

identically at low velocities, at small droplet sizes (< 10 μm) the materials behave identically.

The effect of the solid fraction, as presented in Fig. 9, is interesting because it does not affect the solidification as much as might be expected. It might be for example, 10% solid at impact results in a reduction in size of less than 4%. However, the trend that we can observe numerically is not unexpected, i.e. reducing the amount of liquid reduces the extent that the droplet spreads. This supports our earlier observations that the kinetic energy governs the process. Solidification of the droplet during flight reduces the kinetic energy of the remaining liquid through reducing the volume of liquid. Therefore, with increasing solid fraction, the kinetic energy of liquid decreases leading to a decrease in the spreading extent. It is also interesting to note that the effect of the solid fraction on the decrease in the spreading extent is nearly the same for different materials (the same slopes of lines in Fig. 9). This behaviour further proves that solidification influences the droplet spreading primarily through reducing the liquid volume or mass.

5. Conclusions

Modelling the deformation and solidification of droplets with solid fractions by modifying Madejski's model was successful. We determined that the deformation and solidification depend on the processing conditions, namely the velocity and droplet size, in some fundamental ways. Both the velocity and the droplet size (which determines the mass) contribute directly to the kinetic energy and under LPPS processing conditions the kinetic energy is most important to the deformation and solidification process. The dependence of deformation and solidification on temperature is difficult to define except in general terms relative to the melting point of the material. Furthermore, partial solidification during flight does not effect the deformation and solidification as much as might be expected because of the importance of the kinetic energy.

The properties of the material determine the character of the final dimensions of the solidified droplet. However, the relationship of the properties to the deformation and solidification processes is complex and is influenced by the temperature, making generalizations difficult. Generally, high-density materials flatten substantially more than low-density materials and the temperature sensitivity is determined by the thermal diffusivity. Relatively large thermal diffusivities cause the material to be more sensitive to temperature, especially near the melting temperature. We should also note that the difficulty in determining the properties of the materials can cause perturbations in expected results as demonstrated by the assumptions about the viscosity of tungsten.

Deformation and solidification of a single droplet is not realistically useful except for understanding the processes at work. In real systems involving the accumulation of many solidifying droplets, porosity is an inherent problem. Porosity typically reduces useful properties such as strength and corrosion resistance, degrading the bulk material. Further study is required to gain a firm grasp on how porosity develops in multi-droplet solidification, but we speculate that dense materials accelerated to velocities in the high range ($> 500\ \mathrm{m\,s^{-1}}$) will reduce porosity for two general reasons. Dense materials, such as tungsten, form wider, thinner discs that when stacked have smaller pores or free space; therefore, denser alternatives may produce less porous materials. Higher velocities give liquid droplets more energy to penetrate the pores produced by the stacking of droplets before solidifying; therefore, porosity in less-dense materials may be reduced by accelerating the droplets.

Acknowledgements

We thank Mr P. Lage for the development of the Runge–Kutta scheme and his insight into numerical methods, and Electroplasma Inc., for financial support.

References

1. D. APELIAN, M. PALIWAL, R. W. SMITH and W. F. SCHILLING, *Int. Metals Rev.* **28** (1983) 271.
2. D. WEI, B. FAROUK and D. APELIAN, in "Plasma Processing and Synthesis of Materials", edited by D. Apelian and J. Szekely (Materials Research Society, Pittsburgh, PA, 1987) p. 77.
3. W. LUCAS, "TIG and Plasma Welding – Process Techniques, Recommended Practices and Applications" (Abington, Cambridge, UK, 1990).
4. K. WEBER, *Arc Engng, Stainless Steel* **25** (1989) 12.
5. Flame Coatings PIY Ltd, "Superiors/HVOF Coatings – Higher Particle Velocities Produce Better Thermal Spray Coatings", Internal Report, Sydney, Australia.
6. E. J. LAVERNIA, J. A. AYERS and T. S. SRIVATSAN, *Int. Mater. Rev.* **37** (1992) 1.
7. M. GUPTA, F. A. MOHAMED and E. J. LAVERNIA, *Met. Trans.* **23A** (1992) 831.
8. X. LIANG, J. C. EARTHMAN and E. J. LAVERNIA, *Acta Metall. Mater.*, in press.
9. X. ZENG, H. LIU, M. CHU and E. J. LAVERNIA, *Met. Trans. A*, **23A** (1992) 3394.
10. R. McPHERSON, *Surf. Coat. Technol.* **1** (1989) 173.
11. E. LUGSCHEIDER, and T. WEBER, Fresenius' *Z. Anal. Chem.* **333**, (4–5) I (1989) 293.
12. P. MATHUR, S. ANNAVARAPU, D. APELIAN and A. LAWLEY, *Mater. Sci. Engng* **A142** (1991) 261.
13. R. W. SMITH and D. APELIAN, *Pure Appl. Chem.* **62** (1990) 1825.
14. H. D. STEFFENS, B. WIELAGE and J. DROZAK, *Mater. Wiss. Werkst. Tech.* **21** (1990) 185 (in German).
15. E. J. LAVERNIA, *Int. J. Rapid Solid.* **4** (1988) 89.
16. E. GUTIERRES-MIRAVETE, G. TRAPAGA and J. SZEKELY, in "Casting of Near Net Shape Products", edited by Y. Sahai (The Metallurgical Society, Hawaii 1988).
17. H. LIU, PhD thesis, University of Bremen, FRG (1990) (in German).
18. J. MADEJSKI, *Int. J. Heat Mass Transfer* **19** (1976) 1009.
19. R. D. PHELKE, A. JEYARAJAN and H. WADA "Summary of Thermal Properties for Casting Alloys and Mold Materials" (University of Michigan, Michigan 1982).
20. E. A. BRANDES, "Smithell's Metals Reference Book", 6th Edn (Butterworth, New York, 1983).
21. R. C. WEAST, "CRC Handbook of Chemistry and Physics", 60th Edn (CRC Press, Boca Raton, Florida 1982).

Received 7 September
and accepted 5 November 1992